Probing the Effect of Molecular Nonuniformity in Directed Self-Assembly of Diblock Copolymers in Nanoconfined Space

Louis M. Pitet,[†] Els Alexander-Moonen,[‡] Emiel Peeters,[‡] Tamara S. Druzhinina,[§] Sander F. Wuister,[§] Nathaniel A. Lynd,[∥] and E. W. Meijer*[,†]

[†]Institute for Complex Molecular Systems and Laboratory for Macromolecular and Organic Chemistry, Eindhoven University of Technology, P.O. Box 513, 5600 MB Eindhoven, The Netherlands, [‡]Philips Group Innovation, Research, High Tech Campus 7, 5656 AE Eindhoven, The Netherlands, [§]ASML, De Run 6501, Veldhoven, The Netherlands, and [∥]McKetta Department of Chemical Engineering, University of Texas at Austin, Austin, Texas 78712, United States

ABSTRACT Various complex self-assembled morphologies of lamellar- and cylinder-forming block copolymers comprising poly(dimethylsiloxane)-*b*-polylactide (PDMS-*b*-PLA) confined in cylindrical channels were generated. Combining top-down lithography with bottom-up block copolymer self-assembly grants access to morphologies that are otherwise inaccessible with the bulk materials. Channel diameter (D) was systematically varied with four diblock copolymers having different compositions and bulk domain spacing (L_0), corresponding to a range of frustration ratios (D/L_0 from 2 to 4). Excessive packing frustration imposed by the channels leads to contorted domains. The resulting morphologies depend strongly on both D/L_0 and copolymer composition. Under several circumstances, mixtures of complex morphologies were observed, which hypothetically arise from the severe sensitivity to D/L_0 combined with the inherent compositional/molar mass dispersities associated with the nonuniform synthetic materials and silicon templates. Stochastic calculations offer compelling support for the hypothesis, and tractable pathways toward solving this apparent conundrum are proposed. The materials hold great promise for next-generation nanofabrication to address several emerging technologies, offering significantly enhanced versatility to basic diblock copolymers as templates for fabricating complex nanoscale objects.

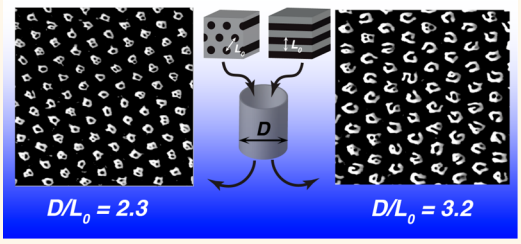

KEYWORDS: block copolymer · nanolithography · confined self-assembly · molecular nonuniformity · bottom-up lithography

Generating discrete nano-objects with complex shapes, intricate internal structure, and versatile chemical functionality has emerged as an intriguing scientific challenge, as the resulting materials have wide-reaching potential across a diverse landscape of advanced technologies including microelectronics, photonics, biosensing, and therapeutics.[1−3] Tremendous progress has been made with block copolymers (BCPs), which typically self-assemble into ordered nanostructures with diverse chemical functionalities. However, with rudimentary block copolymers having two segments—diblock copolymers—one is essentially limited to four distinct bulk morphologies (lamellae, cylinders, gyroid, and spheres).[4−6] Only with more complicated terpolymers and quarterpolymers are complex domain shapes practically accessible under equilibrium bulk conditions.[7−11] Confining block copolymers within nanoscopic voids profoundly influences domain geometry by imposing additional packing frustration that is absent in bulk samples.[12−14] Unfavorable chain stretching leads to structures comprising domains with often contorted geometric configurations and appreciable deviation from bulk equilibrium domain sizes.[15] Simulations using various methods all suggest that diblock copolymers confined in one, two, or three dimensions with boundaries having defined dimensions (D) commensurate with the principal domain spacing (L_0) undergo self-assembly to form an impressively diverse array of unique structures.[16−22]

The combination of top-down (*e.g.*, 193 nm immersion or extreme ultraviolet) with bottom-up (*e.g.*, self-assembly) lithography

* Address correspondence to e.w.meijer@tue.nl.

Received for review October 15, 2014 and accepted August 22, 2015.

Published online September 03, 2015
10.1021/nn505886z

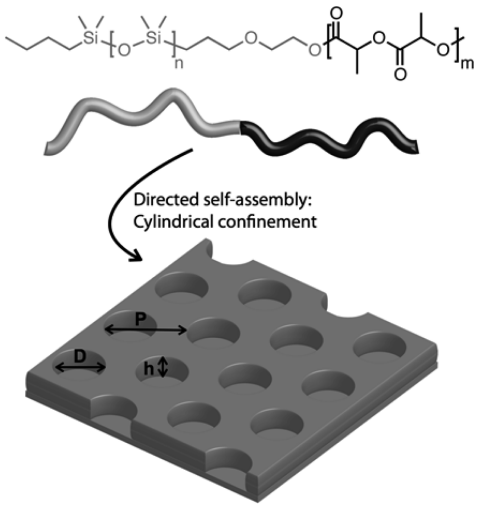

Figure 1. Diblock copolymers of PDMS-*b*-PLA employed in directed self-assembly and an illustrative depiction of the substrate with cylindrical channels for confinement, defined by variable diameter (*D*) and pitch (*P*) and a constant depth (*h*) of 90 nm.

has been accompanied by several technological breakthroughs.[23,24] Conventional photolithography used to fabricate physical barriers on silicon wafers has been explored as directing agents in block copolymer self-assembly.[25−27] For example, dramatic improvement in long-range organization and/or domain alignment has been promoted in shallow trenches.[28−34] Employing circular, square, hexagonal, or other nonlinear confining geometries can induce otherwise energetically costly domain curvature.[35−40] More complex structures have been observed when $D/L_0 \leq 5$ including helices, concentric lamellae, or disorganized arrays by imbibing nanoporous templates with BCPs[41−46] or electrospinning BCP nanofibers.[47,48]

Inspired by the assortment of intricate structures predicted and the ultrasensitivity of those structures to frustration ratios, we employed a diblock copolymer suitable for nanolithography to comprehensively probe the extent to which morphological complexity can be realized under two-dimensional (*i.e.*, cylindrical) confinement at the nanoscale. Furthermore, the effects of molecular nonuniformity on the ability to target specific, narrow-phase windows are experimentally demonstrated and simulated. Utilizing highly immiscible segments—poly(dimethylsiloxane) (PDMS) and poly(D,L-lactide) (PLA)—self-assembled morphologies were investigated for a range of molar masses and compositions (defined by the respective volume fractions, *f*) in cylindrical channels with variable diameter (*D*) from 50 to 100 nm (Figure 1). Owing to the typically strong immiscibility between silicon-containing and aliphatic segments, very small features with sharp interfaces are attainable.[49] Principal domain spacings between 20 and 30 nm were achieved. Additionally, silicon contributes to high etch contrast using standard dry etching techniques (*e.g.*, reactive ion etching).[50]

TABLE 1. Molecular and Morphological Characteristics of PDMS-*b*-PLA Diblock Copolymers

sample	$M_{n,total}$ (kg mol^{-1})[a]	$M_{n,L}$ (kg mol^{-1})[b]	f_L[b]	L_0 (nm)[c]	bulk morphology[d]
[5−4]	9.0	4.0	0.39	21.5	cylinders
[5−8]	12.6	7.6	0.55	19.7	lamellae
[10−7]	16.9	6.9	0.35	28.0	cylinders
[10−13]	22.8	12.8	0.50	30.0	lamellae

[a] Measured by NMR spectroscopy (end-group analysis). [b] Calculated as the volume fraction of PLA at ambient temperature and pressure by assuming the densities of the respective homopolymers ($\rho_D = 0.95$ g/mL; $\rho_L = 1.24$ g/mL). [c] Calculated from the position of the principal peak with the relationship $L_0 = 2\pi/q^*$ for lamellae and $L_0 = 4\pi\sqrt{3}/3q^*$ for cylinders (*i.e.*, cylinder−cylinder distance). [d] Determined as the most likely morphologies based on the allowed Bragg reflections (q/q^*) for the respective space groups. Lamellar: $\sqrt{4}$, $\sqrt{9}$, $\sqrt{16}$, $\sqrt{25}$; hexagonal: $\sqrt{3}$, $\sqrt{4}$, $\sqrt{7}$, $\sqrt{9}$, $\sqrt{12}$, $\sqrt{13}$, $\sqrt{16}$.

PLA was selectively removed to transform the self-assembled morphologies to ornate silica nano-objects. In this way, various hitherto unattainable nanostructures are generated from a conceptually simple set of diblock copolymers combined with industrially established top-down lithographic templates.

RESULTS AND DISCUSSION

PDMS-*b*-PLA diblock copolymers were synthesized by ring-opening polymerization of the cyclic ester D,L-lactide monomer from PDMS macroinitiators (see supplementary files for detailed experimental descriptions). Samples having a range of compositions and molar masses were prepared, with sample names in the format [**X**−**Y**] where **X** and **Y** are the average molar mass of the PDMS and PLA blocks, respectively (Table 1). Equilibrium morphologies under ambient conditions were initially established by small-angle X-ray scattering (SAXS) (see Supporting Information, Figure S1). Samples [**5**−**4**] and [**10**−**7**] both form PLA cylinders hexagonally packed in a PDMS matrix, with corresponding interlayer distances of 18 and 25 nm, respectively. Samples [**5**−**8**] and [**10**−**14**] both adopt alternating lamellae having an average interlayer periodicity of 20 and 30 nm, respectively. The cylinders align parallel to silicon substrates when cast into thin films.[51] The extent of organization was modulated by various annealing procedures, but lattice defects are nonetheless unavoidable in the absence of directing agents.[52]

Polymer solutions were spin-coated onto silicon wafers with cylindrical channels generated with established lithographic techniques (see Supporting Information for wafer preparation description). The channels are arranged in a hexagonal pattern on the wafer; however, the technique allows arbitrary spatial patterns to be generated. Cylinder diameters are systematically varied in the range 50 to 100 nm (±2 nm). The channel depth remained constant at 90 nm. The thermal characteristics of the polymer segments provide a facile route to improve organization and

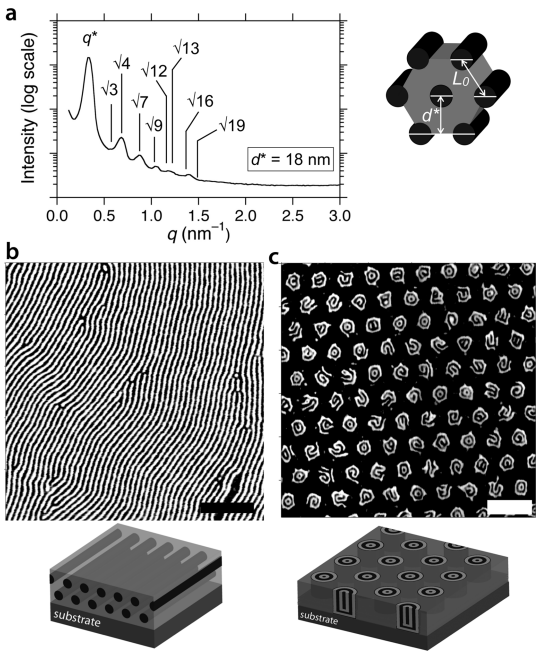

Figure 2. Characteristics of diblock copolymer [5−4] (a) in bulk by SAXS, indicating a morphology containing hexagonally packed cylinders of PLA in a matrix of PDMS; (b) in thin films by SFM (phase image) containing cylinders of PLA lying parallel with the surface; (c) confined in cylindrical channels (D = 80 ± 2 nm; D/L_0 = 4) by SFM (phase image) showing a mixture of morphologies with curved domain interfaces and illustrations showing hypothetical structures throughout the film. Scale bars are 200 nm.

approach thermodynamic equilibrium by thermal annealing at relatively low temperatures (*i.e.*, 100 °C).[51] Annealing 2 h at 100 °C was employed in this study, with no discernible changes observed with longer times/higher temperature. Different morphologies observed by scanning force microscopy (SFM) were found to depend on (1) the composition of the polymer and (2) the ratio D/L_0. The ratios of D/L_0 for the polymers and contact-hole diameters investigated fall between 2.0 and 4.0.

Block copolymer [**5**−**4**] adopts a cylindrical morphology in the bulk (Figure 2a) and in thin films with aligned linear features corresponding to a parallel cylinder orientation, owing to the disparate surface energies of PLA and PDMS (Figure 2b).[51] The image in Figure 2b was captured with SFM after annealing in acetone vapor.

Confining self-assembly can cause stretched chain conformations. A mixture of morphologies, comprised primarily of concentric cylinders (or concentric lamellae) and spirals, is observed at the top surface with [**5**−**4**] in channels having $D = 80 \pm 2$ nm ($D/L_0 = 4$) (Figure 2c). The predominant surface morphology consists of a central dark spot followed by concentric light, dark, and light rings. This is consistent with the surface morphology simulated by various methods for the corresponding ratio of D/L_0 and block polymer composition.[17,19,53] Unambiguously confirming the spatial configuration of domains throughout the pore depth is not possible with SFM alone; for example, cylindrical rings, spirals, and concentric lamellae are all potential conformations. It is impossible to ascertain the domain arrangement and orientation at the bottom of the channels from SFM imaging. The depiction in Figure 2c is entirely hypothetical. For example, both concentric lamellae and stacked doughnuts would likely provide indistinguishable SFM images. Furthermore, neutral wetting at the channel floors is highly unlikely. The disparate surface energies of the blocks suggest a preferential wetting at both the walls and the channel floors. Therefore, the most likely scenario is one in which the walls and floors are covered with the same block, and a corresponding domain contortion is occurring, as suggested by simulations performed previously.[54] We contend that the walls are preferentially wetted by PLA blocks, owing to the low surface energy of PDMS (γ = 20 mJ/mol) and the chemical character of the photoresist employed.[55] However, the wetting layer at the walls is much thinner, comprising compressed chains compared with the bulk domains; therefore, we assume that the layer is not distinguishable in the SFM images.[53]

The image in Figure 2c contains channels that have other morphologies as well (*vide infra*). Some of the different observed structures at the surface by SFM analysis may be different projections of the same morphology. Additionally, several structures have been predicted by self-consistent-field theory to be nearly degenerate in energy. However, the sheer diversity of morphologies observed in the micrograph in Figure 2 cannot be explained by degeneracy. While the simulated morphologies are often very close in energy, the subtle differences between various morphologies is likely a result of molecular composition. Prior to discussing this fascinating anomaly and the implications of molecular nonuniformity, we systematically describe additional samples in various frustration scenarios (*i.e.*, D-variable). Additional samples ultimately indicate the ability to fine-tune a diverse set of complex nanostructures and further show what we infer to be the manifestations of composition dispersity.

The asymmetric copolymer [**10**−**7**] with L_0 = 28 nm adopts various arrangements depending on the confining volume (Figure 3a−d). Nearly exclusively single dark cylinders surrounded by a light ring are observed when D is 60 nm (Figure 3a). The central dark spots most likely consist of PLA; this morphology is approximately consistent with several simulated configurations for cylinder-forming block polymers with the minority component wetting the walls and $D/L_0 \approx 2$.[56] Adoption of a single cylinder running parallel to the channel wall appears likely in a copolymer with asymmetric composition and confining dimensions approximately twice the natural periodicity. A thin compressed layer of PLA probably constitutes the predominant interfacial

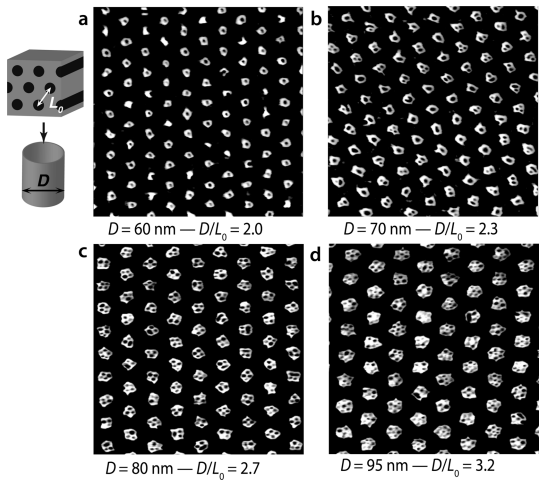

Figure 3. (a–d) SFM images of cylinder-forming block polymer [10–7] with L_0 = 30 nm confined in cylindrical channels having various diameters *D*. Each micrograph is 1 μm × 1 μm.

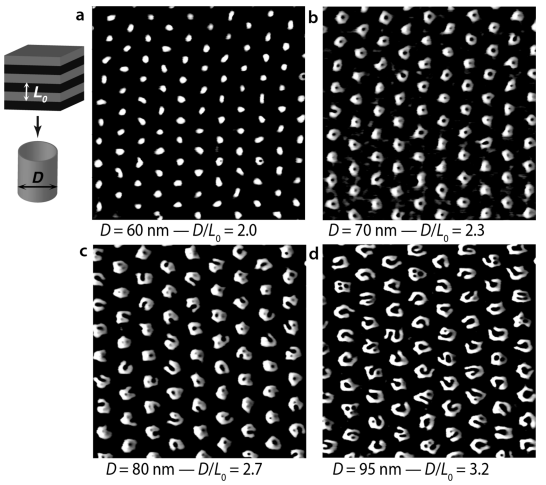

Figure 4. (a–d) SFM images of lamellar-forming block polymer [10–13] with L_0 = 30 nm confined in cylindrical channels having various diameters *D*. Each micrograph is 1 μm × 1 μm.

layer at the wall, as has been simulated for a system with comparable energetic and compositional profile.[56]

A bulk cylinder diameter of 17 nm is measured by SAXS for sample [**10**–**7**], which is slightly larger than that calculated by SFM from the image in Figure 3a (14–17 nm). This suggests slight compression of the PLA chains in the core cylinders when D/L_0 is 2.0. Larger diameter channels (D = 70 nm) result in a mixture of morphologies, with single, double, and triple cylindrical-type structures observed at the surface (Figure 3b). Single cylindrical structures have dimensions appearing substantially dilated compared with the narrower channels. Chain stretching is exacerbated at the central core, leading to average cylinder diameters of approximately 20 nm. Consequently, some channels accommodate the larger volume by adopting two-cylinder-type morphologies (see Figures S2–S9 for additional micrographs, enlarged to accentuate the detailed structures and with phase contrast, *z*-scales, included). Adopting multiple cylinders, with higher average interfacial curvature, is a response to balance the excessive chain stretching that naturally occurs in the dilated domains. The double cylinders are consistently distorted and appear ellipsoidal. Furthermore, some channels have polymer conglomerates adopting triple-cylinder-type structures, with more uniform diameters, albeit significantly compressed and thus smaller than the equilibrium bulk cylinder diameter. Naturally, the three-dimensional domain trajectory is impossible to discern from surface micrographs alone.

Further enlargement of the channel diameter leads to accommodation of additional cylinders, whereby a mixture of three-, four-, and five-cylinder structures are observed with D = 80 nm ($D/L_0 \approx 2.9$; Figure 3c). Yet larger channels provide space to allow seven cylinders to situate and self-assemble in a close-packed hexagonal configuration (Figure 3d). This configuration is particularly intriguing for the manner in which the cylinders are oriented. The polymers essentially adopt a single hexagonal array of the bulk morphology forced into a perpendicular cylinder orientation. Controlled orientation is an important issue for using block copolymer self-assembly for lithographic templates intended for microelectronics and integrated circuits, for example. A great deal of effort is expended to devise strategies to manipulate domain orientation in block copolymer thin films.[57–59]

Changing the molecular composition provides a route to alternate domain configurations, as demonstrated with sample [**10**–**13**] confined in channels of various size (Figure 4a–d). A single light spot is almost exclusively observed when D = 60 nm (D/L_0 = 2.0), comprising most likely a central core domain of PDMS surrounded by a corona of PLA (Figure 4a). The core domains appear asymmetric in the x–y plane. The statistical distribution of orientations of the ellipsoidal core axes suggests that the distortion is real and not merely an artifact. The domain distortion is predicted to become more predominant in bulk-lamellar samples with the chains preferring to adopt flatter interfaces.

Transition to a concentric lamellar structure is observed when D is increased to 70 nm (Figure 4b). This curvature forced onto the domain interface represents a large deviation from the bulk lamellar morphology adopted by this sample and is a conspicuous manifestation of the two-dimensional confinement. Concentric lamellae (with high interfacial curvature) are preferred over a parallel layering of lamellar domains because of the relative surface areas of the walls (A_{wall}) compared with the channel floor (A_{floor}) (*i.e.*, $A_{floor} = (35\text{ nm})^2\pi = 1225\pi\text{ nm}^2$; $A_{wall} = (70\text{ nm}) \times (90\text{ nm})\pi = 6300\pi\text{ nm}^2$). This observation has been predicted in

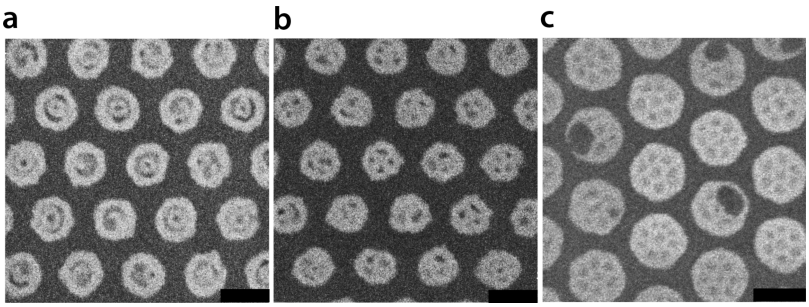

Figure 5. SEM images of different isolated nano-objects from selective dry etching of PLA to afford (a) concentric cylinders, (b) perpendicular three- and four-cylinder-type structures, and (c) hexagonally packed (predominantly) seven-cylinder-type structures. Scale bars are 100 nm.

several simulations of compositionally symmetric, lamellar-forming samples with a strong wetting preference.[19,53,54] The concentric lamellar structure corroborates the strong surface preference for one block; otherwise lamellae oriented perpendicular to the channel axis would be preferred. Further increasing of D to 80 nm results in a mixture of morphologies having relatively complex conformations. The additional interface constraints imposed by the energetic profile of a lamellar sample becomes more apparent when the confining space is slightly larger (Figure 4c). The domain interfaces tend to assume configurations with relatively flat portions combined with more extreme curvature at the bends. The primary morphology in Figure 4c is "e"-shaped. Larger channels (D = 95 nm) facilitate a morphology having several relatively flat interfaces bridged by sharply curved bends, a so-called horseshoe-type morphology (Figure 4d). In addition, the "e"-shaped morphology coexists in Figure 4d. Contorted domain shapes nearly identical to our experimental observations have been simulated with molecular dynamics, albeit with corresponding morphological transitions occurring at different D/L_0 ratios.[16] The difference in transition ratios may be related to relative immiscibility and chain conformations.

The morphologies were transformed into discrete silica nano-objects by selectively etching the PLA domains using standard reactive ion etching. A short fluoro-etch (CHF_3 plasma) was initially employed to remove the thin PDMS wetting layer presumed to cover the air−polymer interface, which was corroborated by contact angle measurements (see Supporting Information for detailed protocol). Scanning electron microscopy (SEM) provides compelling evidence for the removal of PLA and the assigned domains in SFM micrographs depicting the original block polymer templates (Figure 5). For exemplary purposes, we chose three samples with different domain configurations. Figure 5a shows an array of concentric lamellae occurring predominantly. Alternatively, Figure 5b has several channels that appear to have perpendicularly oriented cylindrical recesses that are replicates of the template in Figure 3c. The SEM micrograph, importantly, unambiguously shows a square arrangement of the porous channels; the comparatively distorted, diamond-shaped morphologies in Figure 3c may be an artifact of SFM. Finally, the hexagonal arrays of miniaturized channels were replicated in Figure 5c, demonstrating that a variety of intricate structures can be isolated from the block polymer templates using appropriate etching protocols.

A number of intricate domain configurations have been predicted across a broad range of D/L_0, and our results corroborate several of the simulated morphologies. The experimental observations clearly demonstrate that multiple nanostructures can be fabricated from a single diblock copolymer when confined in channels having dimensions commensurate with the natural bulk periodicity. These complex nanostructures are otherwise inaccessible. Confined self-assembly significantly extends the opportunities for making complicated functional nanostructures with simple and synthetically tractable materials. However, the power of this methodology would be enhanced if individual morphologies could be isolated independently within a given channel array. That is to say, mixed morphologies like that seen in many of the SFM micrographs represent an obstacle to harnessing the potential of this nanofabrication route. We are currently devising strategies for identifying the phenomena that contribute to mixed morphologies.

Simulations performed for various confining geometries have consistently inferred that the adopted nanostructures are severely sensitive to the frustration ratio, D/L_0, with relatively small changes (*ca.* 5%) leading to morphological transitions. Despite the phenomenon of mixed morphologies arising for a given block copolymer having been experimentally observed,[60] this natural impediment toward large-scale nanofabrication employing confined self-assembly has not been specifically addressed. We hypothesize that molar mass dispersity (and consequently compositional dispersity) may contribute substantially to the diversity of observed nanostructures, as mentioned briefly before. For example, a relatively large area micrograph of copolymer [**5**−**8**] in channels with a diameter of 55 nm (*i.e.*, D/L_0 = 2.8) shows a range of morphologies (Figure 6a). Roughly six different morphological

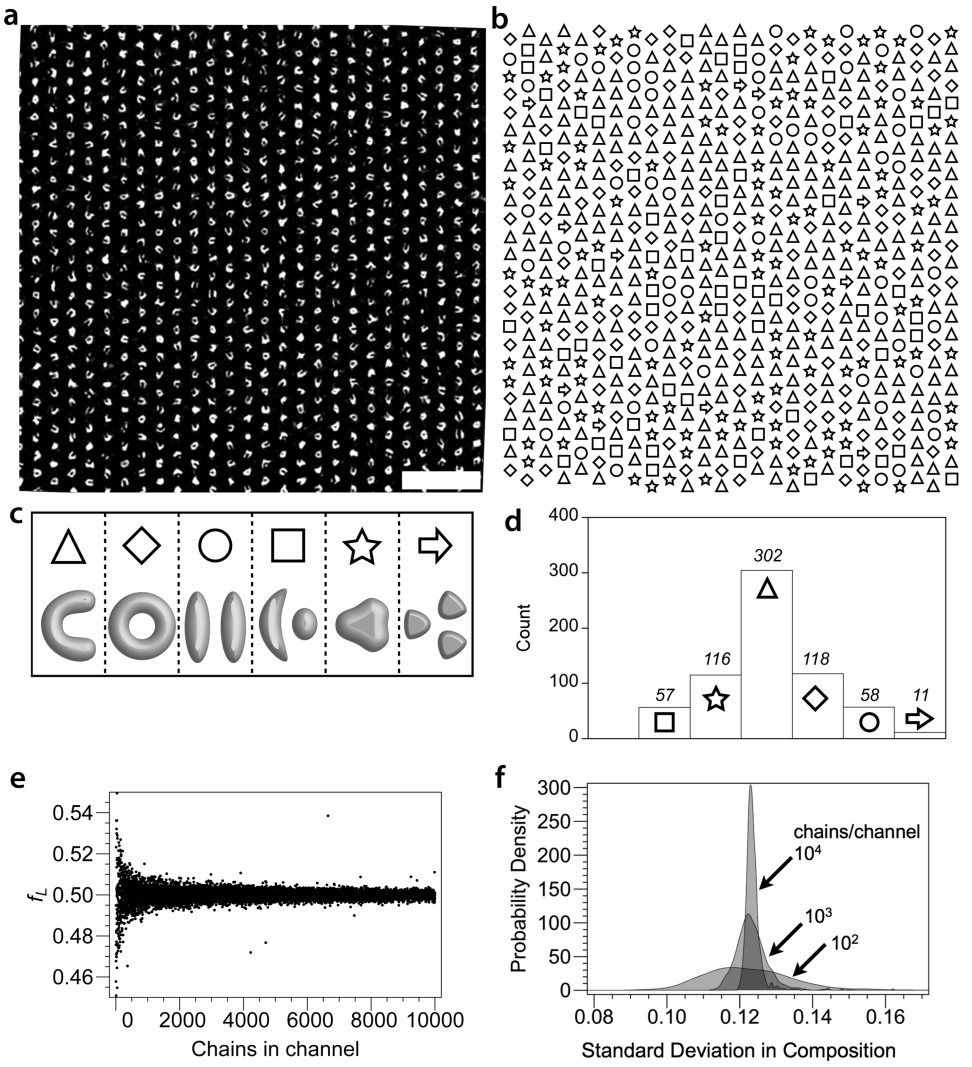

Figure 6. (a) SFM image of lamellar-forming block polymer [5−8] confined in cylindrical channels having diameter $D = 65$ nm. (b) Classification of the different observed morphologies from the SFM image with symbols, with the morphological assignments of the symbols illustrated in (c). (d) Histogram showing the relative abundance of the observed surface morphologies in the single SFM micrograph containing 662 individual channels. Scale bar is 500 nm. (e) Stochastic calculation of average composition per channel as a function of number of chains per channel for a symmetric block polymer with $Đ = 1.1$. (f) Calculated probability density of the standard deviation in composition (using $Đ = 1.1$) for three different values of chains per channel equal to 10^2, 10^3, and 10^4 for a sample of 660 channels corresponding to a typical 2.5 × 2.5 μm^2 SFM field, as shown in part (a).

categories are selected in the micrograph containing 660 individual channels, which are illustrated schematically and assigned an arbitrary shape (*i.e.*, square, circle, triangle, *etc.*, Figure 6b). The different shapes are then mapped onto the original micrograph, providing a coherent visual depiction of the distribution (Figure 6c). Representing the distribution of the nanostructures as a histogram resembles a normal distribution (Figure 6d).

The number of polymer chains within a given channel is estimated to be on the order of 10^3−10^4. Calculating the various average composition and molar mass with respect to the reduced sampling of chains in a single channel clearly suggests that dispersity may cause significant variation between individual channels, which we can surmise would be of consequence to the adopted morphology (Figure 6e). The stochastic evaluation of drift in composition and size reveals that, while most channels are situated close to the ensemble average bulk values, the number of channels having significant deviation is not negligible (see Figure S12). The distribution in average composition and molar mass is pertinently represented by calculating probability densities of the standard deviation distributions as a function of different values of chains per channel (Figure 6f). This shows that indeed there are significant fluctuations in standard deviation, particularly when the number of chains in a channel is small (*e.g.*, 10^2 or 10^3). It remains significant up to 10^4 chains per channel, which falls well within the experimental range. Additional standard deviation distributions are provided for composition and molar mass

(*i.e.*, size) for different samples (Figure S13). All of the samples exhibit similar characteristics, namely, that the drift in composition and size are substantial, even considering modest values of dispersity associated with controlled polymerization techniques that are routinely used in block polymer synthesis. This feature may inevitably be a major contributing factor to the statistical distribution of morphologies observed. The explanation for this comes from the relatively high sensitivity of morphology to the frustration ratio D/L_0. Simulations conducted employing a variety of different methods all exhibit one identical feature: the windows of D/L_0 in which many of the various structures are predicted to be stable are very narrow. Small shifts in composition can lead to correspondingly large changes in L_0 for a fixed molar mass. This is particularly pertinent for the cylindrical morphology (see Figure S14). Furthermore, the lamellar samples [**10**−**13**] and [**5**−**8**] may lie close to the Cyl-Lam boundary owing to the relatively large conformational asymmetry expressed by the PDMS−PLA system.[61]

There are several critical attributes to understanding the implications of the simulations. Most importantly, the variation in size alone, and accordingly dispersity in channel size or wall roughness, does *not* independently suggest that a broad array of morphologies would be produced. However, the molar mass dispersity of each block leads to rather large relative fluctuations in composition, and this characteristic lies at the heart of the proposed explanation for the observed morphological assortment.

According to strong segregation theory, principal domain spacing scales approximately with $N^{2/3}$. Experimentally determined values of $Đ \approx 1.1$ correspond to fluctuation between channels of approximately 5% in N, which translates to even smaller changes in L_0 (based on the $N^{2/3}$ dependence). On the contrary, fluctuations in composition (even at fixed average molar mass) can have exaggerated effects on the characteristic domain spacing (Figure S14).[62,63]

Up to this point, we have ignored any abnormalities or fluctuations in the size or wall roughness in the templates themselves. Naturally, there is a finite distribution of sizes of the channels as well, owing to the photolithographic 193 nm immersion technique employed to fabricate the templates. This dispersity undoubtedly exacerbates the overall fluctuation of composition and molar mass between individual channels and contributes to the distribution of morphologies. These contributions to dispersity are not considered in the calculations. However, for the same reasons outlined above, small size distribution (±2 nm in channel diameter) is not likely to account for the observed fluctuations alone (see additional discussion and example calculations on page S19 of the Supporting Information). A combined picture including wall-surface roughness and channel-size dispersity is beyond the scope of this work and is avidly being pursued for developing this ripe area of directed self-assembly.

CONCLUSION

The implications of molar mass and composition dispersity in block copolymer bulk self-assembly have been extensively explored both experimentally and theoretically.[64−67] However, the role that dispersity may play in dictating conformations in arrays of confined channels and the repercussions on the stochastic distribution of morphologies represent an area that is ripe for additional interrogation. Broad utility of diblock copolymers *via* confined self-assembly has been demonstrated with this work. However, we also establish that alternate polymer synthesis routes may be essential to harness the enormous potential of combining top-down and bottom-up lithography. Nevertheless, employing highly immiscible and silicon-containing components granted ready access to small features that could be transformed into discrete nanoscopic objects through selective etching. Various complex morphologies were generated from block copolymers that are, in bulk, otherwise limited to two simple nanoscale morphologies (lamellae and hexagonally packed cylinders). This work has broad implications for various fields, where the specific shape of functional nanostructures can profoundly impact the resulting physical behavior. This directly demonstrates the promise and limitations of merging lithographic techniques and lends credence to developing equipment capable of increased resolution and line-edge roughness, such as EUV lithography.

These findings point to the need for greater attention being paid to the integrity of the block copolymers *and* the wafers. This becomes exceedingly true in the regime of very low molar mass (and thus correspondingly larger values of Đ, smaller features, and higher immiscibility), which represents an underexplored terrain within confined self-assembly generally. Nearly every report of confined self-assembly uses significantly larger polymers: the behavior and rules are demonstrably different in the limit of low molar mass.

MATERIALS AND METHODS

DL-Lactide was purchased from Sigma-Aldrich and was recrystallized from toluene after azeotropic drying and finally stored in a glovebox under a nitrogen atmosphere. Toluene was dried by stirring over calcium hydride for at least 12 h followed by distillation and stored in a glovebox. Stannous octoate ($Sn(Oct)_2$) was purchased from Sigma-Aldrich and was fractionally distilled using a Kugelrohr apparatus under high vacuum

(~50 mTorr). PDMS monofunctionalized with hydroxyl groups (PDMS-OH) was purchased from Gelest and distributed by Fluorochem Ltd. and was degassed under vacuum for at least 1 h at ambient temperature prior to use. Block copolymers were synthesized from these starting materials in an identical manner to that described previously, with the exception of monomer feed ratios, which were adjusted for targeting different final compositions.[51]

Patterned silicon wafers were generously provided by ASML. The hexagonal patterns were generated by 193 nm immersion lithography. Thin films were prepared by spin-coating polymer solutions onto silicon wafers. Solutions were prepared at 1.0 wt % in HPLC grade heptane, filtered through a 0.2 μm pore size syringe filter, and spun onto the patterned wafers at 2500 rpm. Etching was performed on a custom-built etching instrument housed at Philips High Tech Center, Eindhoven, The Netherlands. Size-exclusion chromatography (SEC) was measured in tetrahydrofuran at 40 °C using a Shimadzu LC system (LC-10AD pump; SIL-10AD autosampler; SPD-M10A diode array detector; RID-10A refractive index detector) containing two high-resolution columns in series (PLgel 5 μm Mixed C and PLgel 5 μm Mixed D columns). Bulk SAXS was performed on an instrument from Ganesha Lab. SFM was performed with an Asylum Research MFP 3D microscope equipped with an anti-vibration table and housed in an insulated chamber. SEM was performed on an XL50 SFEG from FEI, operating at an accelerating voltage of 10 keV, spot size of 3, and working distance of 5.2 mm. Samples were imaged directly on silicon wafers after etching, with no additional processing (*e.g.*, coating) applied.

Conflict of Interest: The authors declare no competing financial interest.

Acknowledgment. The authors gratefully acknowledge funding (L.M.P. and E.W.M.) from the Ministry of Education, Culture, and Science (Gravity Program 024.001.035), The Netherlands Organization for Scientific Research (NWO), the European Research Council (FP7/2007-2013), and ERC Grant Agreement 246829.

Supporting Information Available: The Supporting Information is available free of charge on the ACS Publications website at DOI: 10.1021/nn505886z.

Additional experimental details, SAXS data, additional SFM phase and height images, comprehensive statistical simulations for the different samples, script to perform related simulations (PDF)

REFERENCES AND NOTES

1. Suteewong, T.; Sai, H.; Hovden, R.; Muller, D.; Bradbury, M. S.; Gruner, S. M.; Wiesner, U. Multicompartment Mesoporous Silica Nanoparticles with Branched Shapes: An Epitaxial Growth Mechanism. *Science* **2013**, *340*, 337–341.
2. Petros, R. A.; DeSimone, J. M. Strategies in the Design of Nanoparticles for Therapeutic Applications. *Nat. Rev. Drug Discovery* **2010**, *9*, 615–627.
3. Biswas, A.; Bayer, I. S.; Biris, A. S.; Wang, T.; Dervishi, E.; Faupel, F. Advances in Top-Down and Bottom-up Surface Nanofabrication: Techniques, Applications & Future Prospects. *Adv. Colloid Interface Sci.* **2012**, *170*, 2–27.
4. Bates, F. S.; Fredrickson, G. H. Block Copolymer Thermodynamics: Theory and Experiment. *Annu. Rev. Phys. Chem.* **1990**, *41*, 525–557.
5. Takenaka, M.; Wakada, T.; Akasaka, S.; Nishitsuji, S.; Saijo, K.; Shimizu, H.; Kim, M. I.; Hasegawa, H. Orthorhombic Fddd Network in Diblock Copolymer Melts. *Macromolecules* **2007**, *40*, 4399–4402.
6. Tyler, C. A.; Morse, D. C. Orthorhombic Fddd Network in Triblock and Diblock Copolymer Melts. *Phys. Rev. Lett.* **2005**, *94*, 208302.
7. Walther, A.; Muller, A. H. E. Janus Particles: Synthesis, Self-Assembly, Physical Properties, and Applications. *Chem. Rev.* **2013**, *113*, 5194–5261.
8. Matsushita, Y.; Takano, A.; Hayashida, K.; Asari, T.; Noro, A. Hierarchical Nanophase-Separated Structures Created by Precisely-Designed Polymers with Complexity. *Polymer* **2009**, *50*, 2191–2203.
9. Stadler, R.; Auschra, C.; Beckmann, J.; Krappe, U.; Voight-Martin, I.; Leibler, L. Morphology and Thermodynamics of Symmetric Poly(A-Block-B-Block-C) Triblock Copolymers. *Macromolecules* **1995**, *28*, 3080–3097.
10. Hadjichristidis, N.; Pitsikalis, M.; Iatrou, H. Synthesis of Block Copolymers. *Adv. Polym. Sci.* **2005**, *189*, 1–124.
11. Bates, F. S.; Hillmyer, M. A.; Lodge, T. P.; Bates, C. M.; Delaney, K. T.; Fredrickson, G. H. Multiblock Polymers: Panacea or Pandora's Box? *Science* **2012**, *336*, 434–440.
12. Lambooy, P.; Russell, T. P.; Kellogg, G. J.; Mayes, A. M.; Gallagher, P. D.; Satija, S. K. Observed Frustration in Confined Block Copolymers. *Phys. Rev. Lett.* **1994**, *72*, 2899–2902.
13. Shin, K.; Xiang, H. Q.; Moon, S. I.; Kim, T.; McCarthy, T. J.; Russell, T. P. Curving and Frustrating Flatland. *Science* **2004**, *306*, 76–76.
14. Ma, M. L.; Thomas, E. L.; Rutledge, G. C.; Yu, B.; Li, B. H.; Jin, Q. H.; Ding, D. T.; Shi, A. C. Gyroid-Forming Diblock Copolymers Confined in Cylindrical Geometry: A Case of Extreme Makeover for Domain Morphology. *Macromolecules* **2010**, *43*, 3061–3071.
15. Yabu, H.; Higuchi, T.; Jinnai, H. Frustrated Phases: Polymeric Self-Assemblies in a 3d Confinement. *Soft Matter* **2014**, *10*, 2919–2931.
16. Park, J. H.; Kalra, V.; Joo, Y. L. Cylindrically Confined Assembly of Asymmetrical Block Copolymers with and without Nanoparticles. *Soft Matter* **2012**, *8*, 1845–1857.
17. Yu, B.; Sun, P. C.; Chen, T. H.; Jin, Q. H.; Ding, D. T.; Li, B. H.; Shi, A. C. Confinement-Induced Novel Morphologies of Block Copolymers. *Phys. Rev. Lett.* **2006**, *96*, 138306.
18. Yu, B.; Li, B. H.; Jin, Q. H.; Ding, D. T.; Shi, A. C. Confined Self-Assembly of Cylinder-Forming Diblock Copolymers: Effects of Confining Geometries. *Soft Matter* **2011**, *7*, 10227–10240.
19. Pinna, M.; Guo, X. H.; Zvelindovsky, A. V. Diblock Copolymers in a Cylindrical Pore. *J. Chem. Phys.* **2009**, *131*, 214902-1–214902-7.
20. Sevink, G. J. A.; Zvelindovsky, A. V. Block Copolymers Confined in a Nanopore: Pathfinding in a Curving and Frustrating Flatland. *J. Chem. Phys.* **2008**, *128*, 084901.
21. Li, W.; Wickham, R. A.; Garbary, R. A. Phase Diagram for a Diblock Copolymer Melt under Cylindrical Confinement. *Macromolecules* **2006**, *39*, 806–811.
22. Shi, A. C.; Li, B. H. Self-Assembly of Diblock Copolymers under Confinement. *Soft Matter* **2013**, *9*, 1398–1413.
23. Bang, J.; Jeong, U.; Ryu, D. Y.; Russell, T. P.; Hawker, C. J. Block Copolymer Nanolithography: Translation of Molecular Level Control to Nanoscale Patterns. *Adv. Mater.* **2009**, *21*, 4769–4792.
24. Cheng, J. Y.; Ross, C. A.; Smith, H. I.; Thomas, E. L. Templated Self-Assembly of Block Copolymers: Top-Down Helps Bottom-Up. *Adv. Mater.* **2006**, *18*, 2505–2521.
25. Koo, K.; Ahn, H.; Kim, S.-W.; Ryu, D. Y.; Russell, T. P. Directed Self-Assembly of Block Copolymers in the Extreme: Guiding Microdomains from the Small to the Large. *Soft Matter* **2013**, *9*, 9059–9071.
26. Yang, J. K. W.; Jung, Y. S.; Chang, J. B.; Mickiewicz, R. A.; Alexander-Katz, A.; Ross, C. A.; Berggren, K. K. Complex Self-Assembled Patterns Using Sparse Commensurate Templates with Locally Varying Motifs. *Nat. Nanotechnol.* **2010**, *5*, 256–260.
27. Chang, J. B.; Son, J. G.; Hannon, A. F.; Alexander-Katz, A.; Ross, C. A.; Berggren, K. K. Aligned Sub-10-nm Block Copolymer Patterns Templated by Post Arrays. *ACS Nano* **2012**, *6*, 2071–2077.
28. Segalman, R. A.; Yokoyama, H.; Kramer, E. J. Graphoepitaxy of Spherical Domain Block Copolymer Films. *Adv. Mater.* **2001**, *13*, 1152–1155.
29. Park, S. M.; Stoykovich, M. P.; Ruiz, R.; Zhang, Y.; Black, C. T.; Nealey, P. E. Directed Assembly of Lamellae-Forming Block Copolymers by Using Chemically and Topographically Patterned Substrates. *Adv. Mater.* **2007**, *19*, 607–611.
30. Jeong, S. J.; Moon, H. S.; Kim, B. H.; Kim, J. Y.; Yu, J.; Lee, S.; Lee, M. G.; Choi, H.; Kim, S. O. Ultralarge-Area Block

Copolymer Lithography Enabled by Disposable Photoresist Prepatterning. *ACS Nano* **2010**, *4*, 5181–5186.
31. Kim, E.; Ahn, H.; Park, S.; Lee, H.; Lee, M.; Lee, S.; Kim, T.; Kwak, E. A.; Lee, J. H.; Lei, X.; et al. Directed Assembly of High Molecular Weight Block Copolymers: Highly Ordered Line Patterns of Perpendicularly Oriented Lamellae with Large Periods. *ACS Nano* **2013**, *7*, 1952–1960.
32. Keen, I.; Cheng, H. H.; Yu, A. G.; Jack, K. S.; Younkin, T. R.; Leeson, M. J.; Whittaker, A. K.; Blakey, I. Behavior of Lamellar Forming Block Copolymers under Nanoconfinement: Implications for Topography Directed Self-Assembly of Sub-10 Nm Structures. *Macromolecules* **2014**, *47*, 276–283.
33. Kim, S.; Shin, D. O.; Choi, D. G.; Jeong, J. R.; Mun, J. H.; Yang, Y. B.; Kim, J. U.; Kim, S. O.; Jeong, J. H. Graphoepitaxy of Block-Copolymer Self-Assembly Integrated with Single-Step Zno Nanoimprinting. *Small* **2012**, *8*, 1563–1569.
34. Berry, B. C.; Singh, G.; Kim, H. C.; Karim, A. Highly Aligned Block Copolymer Thin Films by Synergistic Coupling of Static Graphoepitaxy and Dynamic Thermal Annealing Fields. *ACS Macro Lett.* **2013**, *2*, 346–350.
35. Yamaguchi, T.; Yamaguchi, H. Two-Dimensional Patterning of Flexible Designs with High Half-Pitch Resolution by Using Block Copolymer Lithography. *Adv. Mater.* **2008**, *20*, 1684–1689.
36. Jung, Y. S.; Jung, W.; Ross, C. A. Nanofabricated Concentric Ring Structures by Templated Self-Assembly of a Diblock Copolymer. *Nano Lett.* **2008**, *8*, 2975–2981.
37. Wilmes, G. M.; Durkee, D. A.; Balsara, N. P.; Liddle, J. A. Bending Soft Block Copolymer Nanostructures by Lithographically Directed Assembly. *Macromolecules* **2006**, *39*, 2435–2437.
38. Park, S.-M.; Dong, M.; Rettner, C. T.; Dandy, D. S.; Wang, Q.; Kim, H.-C. Bending of Lamellar Microdomains of Block Copolymers on Nonselective Surfaces. *Macromolecules* **2010**, *43*, 1665–1670.
39. Hong, S. W.; Gu, X. D.; Huh, J.; Xiao, S. G.; Russell, T. P. Circular Nanopatterns over Large Areas from the Self-Assembly of Block Copolymers Guided by Shallow Trenches. *ACS Nano* **2011**, *5*, 2855–2860.
40. Chai, J.; Buriak, J. M. Using Cylindrical Domains of Block Copolymers to Self-Assemble and Align Metallic Nanowires. *ACS Nano* **2008**, *2*, 489–501.
41. Jones, B. H.; Lodge, T. P. Hierarchically Structured Materials from Block Polymer Confinement within Bicontinuous Microemulsion-Derived Nanoporous Polyethylene. *ACS Nano* **2011**, *5*, 8914–8927.
42. Wu, Y. Y.; Cheng, G. S.; Katsov, K.; Sides, S. W.; Wang, J. F.; Tang, J.; Fredrickson, G. H.; Moskovits, M.; Stucky, G. D. Composite Mesostructures by Nano-Confinement. *Nat. Mater.* **2004**, *3*, 816–822.
43. Xiang, H.; Shin, K.; Kim, T.; Moon, S. I.; McCarthy, T. J.; Russell, T. P. Block Copolymers under Cylindrical Confinement. *Macromolecules* **2004**, *37*, 5660–5664.
44. Dobriyal, P.; Xiang, H. Q.; Kazuyuki, M.; Chen, J. T.; Jinnai, H.; Russell, T. P. Cylindrically Confined Diblock Copolymers. *Macromolecules* **2009**, *42*, 9082–9088.
45. Xiang, H.; Shin, K.; Kim, T.; Moon, S. I.; McCarthy, T. J.; Russell, T. P. From Cylinders to Helices Upon Confinement. *Macromolecules* **2005**, *38*, 1055–1056.
46. Arsenault, A. C.; Rider, D. A.; Tetreault, N.; Chen, J. I. L.; Coombs, N.; Ozin, G. A.; Manners, I. Block Copolymers under Periodic, Strong Three-Dimensional Confinement. *J. Am. Chem. Soc.* **2005**, *127*, 9954–9955.
47. Ma, M.; Krikorian, V.; Yu, J. H.; Thomas, E. L.; Rutledge, G. C. Electrospun Polymer Nanofibers with Internal Periodic Structure Obtained by Microphase Separation of Cylindrically Confined Block Copolymers. *Nano Lett.* **2006**, *6*, 2969–2972.
48. Kalra, V.; Mendez, S.; Lee, J. H.; Nguyen, H.; Marquez, M.; Joo, Y. L. Confined Assembly in Coaxially Electrospun Block-Copolymer Fibers. *Adv. Mater.* **2006**, *18*, 3299–3303.
49. Nunns, A.; Gwyther, J.; Manners, I. Inorganic Block Copolymer Lithography. *Polymer* **2013**, *54*, 1269–1284.
50. Ross, C. A.; Jung, Y. S.; Chuang, V. P.; Ilievski, F.; Yang, J. K. W.; Bita, I.; Thomas, E. L.; Smith, H. I.; Berggren, K. K.; Vancso, G. J.; et al. Si-Containing Block Copolymers for Self-Assembled Nanolithography. *J. Vac. Sci. Technol., B* **2008**, *26*, 2489–2494.
51. Pitet, L. M.; Wuister, S.; Peeters, E.; Hawker, C. J.; Kramer, E. J.; Meijer, E. W. Well-Organized Dense Arrays of Nanodomains in Thin-Films of Poly(Dimethylsiloxane)-b-Poly(Lactide) Diblock Copolymers. *Macromolecules* **2013**, *46*, 8289–8295.
52. Mishra, V.; Fredrickson, G. H.; Kramer, E. J. Effect of Film Thickness and Domain Spacing on Defect Densities in Directed Self-Assembly of Cylindrical Morphology Block Copolymers. *ACS Nano* **2012**, *6*, 2629–2641.
53. Yu, B.; Sun, P. C.; Chen, T. H.; Jin, Q. H.; Ding, D. T.; Li, B. H.; Shi, A. C. Self-Assembly of Diblock Copolymers Confined in Cylindrical Nanopores. *J. Chem. Phys.* **2007**, *127*, 114906.
54. Laachi, N.; Delaney, K. T.; Kim, B.; Hur, S.-M.; Bristol, R.; Shykind, D.; Weinheimer, C. J.; Fredrickson, G. H. Self-Consistent Field Theory Investigation of Directed Self-Assembly in Cylindrical Confinement. *J. Polym. Sci., Part B: Polym. Phys.* **2015**, *53*, 142–153.
55. Jung, Y. S.; Ross, C. A. Orientation-Controlled Self-Assembled Nanolithography Using a Polystyrene-Polydimethylsiloxane Block Copolymer. *Nano Lett.* **2007**, *7*, 2046–2050.
56. Chen, P.; Liang, H. J.; Shi, A. C. Origin of Microstructures from Confined Asymmetric Diblock Copolymers. *Macromolecules* **2007**, *40*, 7329–7335.
57. Mansky, P.; Liu, Y.; Huang, E.; Russell, T. P.; Hawker, C. J. Controlling Polymer-Surface Interactions with Random Copolymer Brushes. *Science* **1997**, *275*, 1458–1460.
58. Hong, S. W.; Voronov, D. L.; Lee, D. H.; Hexemer, A.; Padmore, H. A.; Xu, T.; Russell, T. P. Controlled Orientation of Block Copolymers on Defect-Free Faceted Surfaces. *Adv. Mater.* **2012**, *24*, 4278–4283.
59. Kim, S. H.; Misner, M. J.; Russell, T. P. Controlling Orientation and Order in Block Copolymer Thin Films. *Adv. Mater.* **2008**, *20*, 4851–4856.
60. Higuchi, T.; Tajima, A.; Motoyoshi, K.; Yabu, H.; Shimomura, M. Frustrated Phases of Block Copolymers in Nanoparticles. *Angew. Chem., Int. Ed.* **2008**, *47*, 8044–8046.
61. Matsen, M. W.; Bates, F. S. Block Copolymer Microstructures in the Intermediate-Segregation Regime. *J. Chem. Phys.* **1997**, *106*, 2436–2448.
62. Matsushita, Y.; Noro, A.; Iinuma, M.; Suzuki, J.; Ohtani, H.; Takano, A. Effect of Composition Distribution on Microphase-Separated Structure from Diblock Copolymers. *Macromolecules* **2003**, *36*, 8074–8077.
63. Noro, A.; Iinuma, M.; Suzuki, J.; Takano, A.; Matsushita, Y. Effect of Composition Distribution on Microphase-Separated Structure from BAB Triblock Copolymers. *Macromolecules* **2004**, *37*, 3804–3808.
64. Lynd, N. A.; Meuler, A. J.; Hillmyer, M. A. Polydispersity and Block Copolymer Self-Assembly. *Prog. Polym. Sci.* **2008**, *33*, 875–893.
65. Matsen, M. W. Effect of Large Degrees of Polydispersity on Strongly Segregated Block Copolymers. *Eur. Phys. J. E: Soft Matter Biol. Phys.* **2006**, *21*, 199–207.
66. Noro, A.; Cho, D.; Takano, A.; Matsushita, Y. Effect of Molecular Weight Distribution on Microphase-Separated Structures from Block Copolymers. *Macromolecules* **2005**, *38*, 4371–4376.
67. Schmitt, A. K.; Mahanthappa, M. K. Characteristics of Lamellar Mesophases in Strongly Segregated Broad Dispersity ABA Triblock Copolymers. *Macromolecules* **2014**, *47*, 4346–4356.